



Investigation of Nano- Al_2O_3 and Micro-coconut Shell Ash (CSA) Reinforced AA7075 Hybrid Metal–Matrix Composite Using Two-Stage Stir Casting

Ashish Kumar^{1,2} · R. C. Singh¹ · Rajiv Chaudhary¹

Received: 10 August 2021 / Accepted: 17 February 2022 / Published online: 11 March 2022
© King Fahd University of Petroleum & Minerals 2022

Abstract

The present work is focused on the influences of reinforced particles on mechanical, microstructural, and tribological performances of AA7075 hybrid metal–matrix composites (HMMCs). Al_2O_3 and coconut shell ash (CSA) were reinforced using two-stage stir casting by varying the wt% (0–5) of reinforcement. Microstructural analysis and various phase identifications were examined with the help of scanning electron microscope (SEM) equipped with EDX and optical microscope. Various mechanical testing such as tensile, hardness, 3-point bend test, and tribological behaviors were carried out to know the HMMCs properties. Microstructural images revealed a homogeneous distribution of reinforced particles in the metal–matrix and EDX confirmed the presence of dispersed reinforcements (Al_2O_3 and CSA) in the HMMCs. It was seen that mechanical properties and tribological behavior have been increased after addition of Al_2O_3 and CSA reinforced particles whereas slightly decreased in impact strength. Transgranular cleavage facets, micro-void coalescence, dimples, and crack were shown in SEM images of fractured specimens during impact and tensile testing.

Keywords AA7075 · Al_2O_3 · Coconut shell ash (CSA) · Stir casting · Microstructure · Mechanical properties · Flexural test

1 Introduction

Al-alloys have its own inherent properties such as good mechanical strength, low density, and excellent corrosion resistance, and it leads to a widespread application in automobile and aerospace industries [1]. Particularly AA7075 alloy is a cold-finished wrought product having zinc as a primary alloying element. It has the highest tensile strength among all Al-screw machine alloys. AA7075 alloy is used for the highly stressed structural components including aircraft fitting, shafts, gear, and a variety of other commercial aircraft, transportations, and equipment [2]. Generally, the Al-alloys strength can be enhanced in various means, including: (i) by the addition of insoluble second particles to form hybrid metal–matrix composite (HMMCs) [3], (ii) by the

precipitation hardening method [4], (iii) by the surface coatings method, (iv) by the cryogenic treatments method, etc. [5]. Among the above-mentioned processes, HMMCs contain much concentration in improving the tribological and mechanical properties of aluminum. A metal composite is generally made up of two or more than two insoluble phase particles. Comparing the base constituents material, HMMCs have better properties in various aspects. Since it is easily fabricable, low density, and superior engineering properties, aluminum and its alloys are preferably chosen to be as the matrix material in majority conditions [6]. Typically, the Al-MMCs are processed under (i) Liquid-state (pressurized die casting, stir casting, infiltration process), (ii) solid-state (diffusion bonding, physical-vapor deposition (PVD), and powder metallurgy (PM)), and (iii) in situ dispensation. Researchers suggested that the stir casting is the helpful and most effective route among these mentioned procedures. Prior to the production of HMMCs, several crucial set of parameters such as stirring time and speed, melting temperature, holding or dwell time, stirring position, die preheating, and insoluble second particles can be deliberated. The properties of developed composite are decided by the optimum selection of mentioned parameters [7–13].

✉ Ashish Kumar
ashuatcoer@gmail.com

¹ Department of Mechanical Engineering, Delhi Technological University, Delhi 110042, India

² Department of Mechanical Engineering, Galgotias College of Engineering and Technology, Greater Noida 201306, India



The evolution of Al-HMMCs can be categorized into distinct stages. First stage: The properties of Al-matrix are improved by addition of single solid reinforced particle. The continuous and discontinuous category of solid reinforced particle can be continuous fibers such as SiC fiber and carbon fiber and discontinuous such as whiskers, short fiber, and particles. Among the above-mentioned category, particle reinforced Al-HMMCs are used broadly. In this category the most commonly used reinforced ceramic particles such as B_4C , SiC, and TiC, oxides such as MgO, Al_2O_3 , ZrO_2 , nitrides such as AlN and BN, whereas borides such as TiB_2 and AlB_2 , are used as second particle with the Al-alloy [14–16]. Second stage: Hybrid Al MMCs were introduced to improve the HMMCs properties compared to single-solid reinforced particle. The hybrid metal–matrix composite (HMMCs) is the addition of more than one synthetic ceramic particle in the aluminum matrix. It is measured as a better result than has been proved in the second stage [17, 18]. Third stage: Industrial waste is used to utilize with better properties of HMMCs, the industrial waste, and synthetic ceramic-like graphite, fly ash, red mud, and cow dung ash, coconut shell ash, etc., are added and superior outcome have been reported [19–21].

A number of investigations have confirmed that the ultimate tensile strength (UTS) and hardness of AA7075 reinforced with nano- Al_2O_3 particles enhanced dramatically with increase in weight % of Al_2O_3 . The nano-ceramic particles when used as reinforcement, it strengthens the matrix with good ductility. The composting method was developed to fabricate nano-SiC or Al_2O_3 reinforced Al-alloy composites [7, 11, 22]. The present scenarios in the development of Al-based HMMCs are reinforcing agriculture waste with ceramic particles. Agriculture waste such as rice husk ash, bamboo leaf ash, bagasse ash, maize stalk ash, palm kernel ash, and corn cob ash are used and superior properties have been obtained [7, 20, 21, 23].

The two or more synthetic ceramics particles in matrix including the main drawbacks are it increases brittleness and reduces ductility in composites materials. Because of the increased brittle nature of composite, the surface roughness is affected by machining characteristics; moreover, weight of the composite enhances because of the variation in the density between matrix and particles. Generally, the artificial ceramics particles are shown brittle behavior and frequently employed as abrasives particle wherever the cost is higher. The agriculture litters or wastes are one of the hopeful substitutes to overcome the above-mentioned drawbacks. Coconut shell ash consists of silicon oxide, alumina, iron oxides, magnesium oxide, etc., which would improve the properties of base metal. The major profits of CSA are less density, low cost, and also reduced pollution [23–26]. The hybrid composite consists of B_4C , and coconut shell ash improves its properties like tensile, hardness, and a minimum level of

porosity present. Dimple fracture form is shown during the tensile test [27]. Hence, a challenge has been made in CSA as the second reinforcement in Al-based MMCs. AA7075 is commonly identified as high tensile strength-to-weight ratio which is utilized in aeronautical, electronic, and automotive uses. The main components of automobile like brake calipers, piston, rocker arms, and wheels are manufactured using AA7075 alloy [28].

In the present work, the weight % of Al_2O_3 and CSA reinforced particles are varied and the mechanical properties like impact strength, ultimate tensile strength (UTS), hardness, flexural strength, and compressive strength are evaluated. Further tribological behaviors are evaluated for the fabricated specimen. The existence of compounds and distribution of second-phase particles in metal–matrix are observed with optical metallographic (OM) and SEM equipped with EDX respectively.

2 Experimental Procedure

2.1 Material Selection

AA7075 alloys are chosen as a base material (matrix) in the form of small size sheet and rod. Spectro analysis is done for chemical analysis and the compositions of a matrix (AA7075) are listed in Table 1. The average size of 50 nm of Al_2O_3 and micro-size coconut shell ash (CSA) is used as reinforcement shown in Fig. 1. Coconut shell is collected in a container and carefully dried in the daylight for four days to eliminate the moisture. The coconut shell is crushed into fine pieces and further burn in open furnace to make ash. The fine ash particle is collected in a container and heated for 3 h at 620 °C in a muffle furnace to abolish carbonaceous particles present in CSA. Various elements and compounds exist in CSA are listed in Table 2. The particle size was screened in the sieving machine to verify the estimated range of CSA size. The particle size of Al_2O_3 is in nano-range and CSA ranging average of 50–70 μm are used in this study. The confirmation of nano- Al_2O_3 particles was validated by TEM analysis.

2.2 Fabrication Process

Aluminum HMMCs were developed by the stir casting method as shown Fig. 2, whereas pure aluminum powder (μm) and Al_2O_3 powder (nm) were intermixed and added to injection molding machine after compression of the powder form into a circular disk-shape block as shown in Fig. 3. The Al- Al_2O_3 -CSA hybrid MMCs were melted in the electric furnace. The Al matrix heated till melting start and further cooled at slurry stage and mixed well manually in two-stage stir casting. The desired temperature is achieved when the

Table 1 Spectro analysis of AA7075 alloy

AA7075	Zn	Mg	Fe	Cu	Fe	Cr	Ti	Si	Al
Weight %	5.49	2.45	0.41	1.43	0.13	0.21	0.12	0.13	Balance

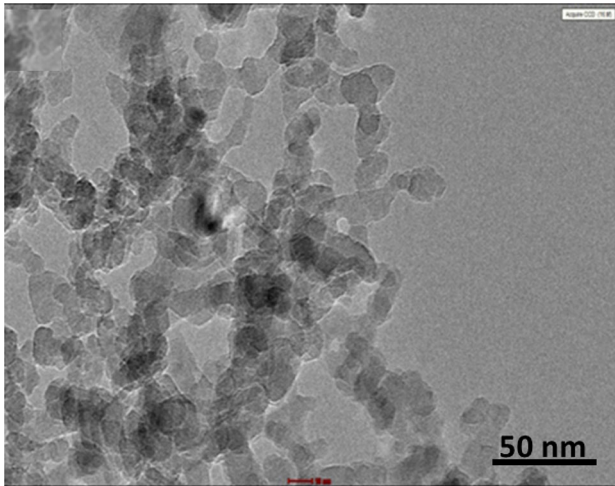


Fig.1 TEM analysis of nano-alumina powder

slurry is further heated and the matrix is stirred by mechanical stirrer. The main advantages of this stir casting over conventional stir casting process are the particles that were spread all over the matrix to obtain a homogeneous dispersion of the

reinforcement [15]. The optimum stir casting process parameters are mentioned in Table 3. The muffle furnace is used to preheat the reinforcement for 2.5 h to remove the absorbed volatile contents. A graphite crucible is used to melt pure Al 7075 alloy about 1.5 kg per sample. AA7075 is heated in two-stage casting up to melting temperature and further cool at the semisolid state. At this state, preheated alumina and CSA particles are mixed well for 5–6 min. After that the molten slurry is then heated up to 950 °C for dissimilar weight % of reinforced particle which is shown in Table 4. The weight percentage of sample N0, N1, N2, and N3 were selected based on the existing literature and experimental analysis. By keeping both one as constant, the result was not much affected and hence percentage of both reinforcements was increased in research. Once the melt temperature has achieved 950 °C, liquid slurry is stirred with the help of four blades mechanical stirrer rotated in the range of (350–450 rpm) for 5–7 min to make a uniform distribution of reinforcement in composite material.

Table 2 XRF Oxide analysis of CSA

CSA	SiO ₂	Al ₂ O ₃	Fe ₂ O ₃	MgO	Na ₂ O	CaO	ZnO	MnO
Weight %	45.35	21.85	18.60	12.35	0.75	0.68	0.31	0.21

Fig.2 Stir casting process mechanism

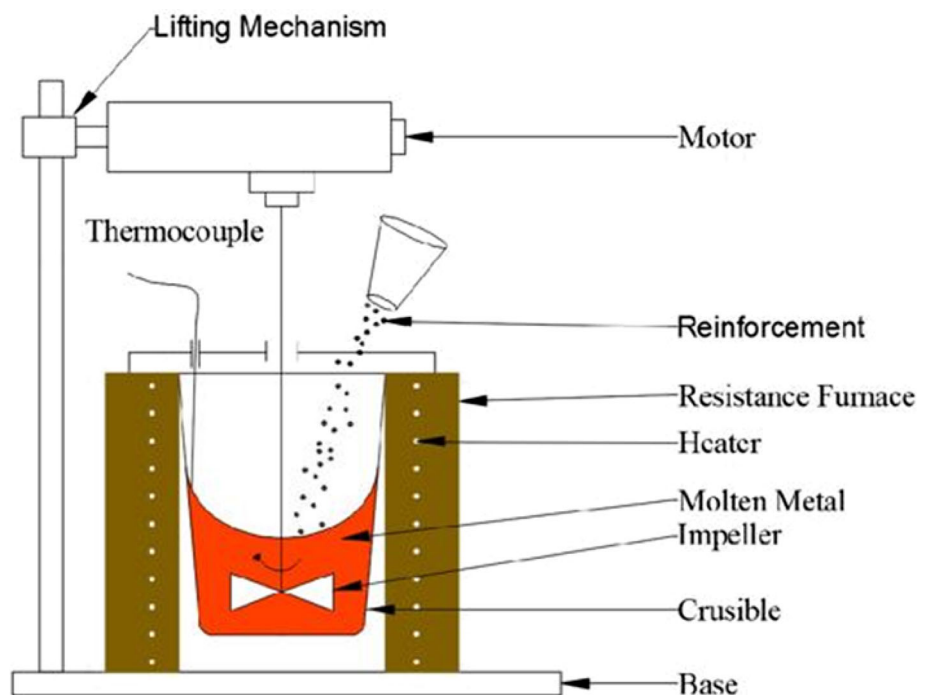




Fig.3 Preparation of powder (Pure Al + nano-alumina)

Table 3 Stir casting process parameter

Process parameter	Selected parameter
Mold preheat temperature	280 °C
Processing temperature	950 °C
Preheat temperature of reinforcement	350 °C
Stirring speed	350 RPM
Stirring time	5 min
Blade angle	45°
Position of stirrer	Up to 75% of depth

Table 4 Percentage of reinforcements

Sample	Nano-size Al ₂ O ₃ (wt.%) (%)	Micro-size CSA (wt.%) (%)	AA7075 (wt.%)
N0	0	0	100%
N1	0.2	1	Remaining
N2	0.4	2	Remaining
N3	0.6	3	Remaining

2.3 Microstructural Characterization

Different specimens having dimensions (10 mm × 10 mm × 10 mm) were machined and after that standard polishing with various grades, i.e., 500, 800, 1000, 1500, 2000, of emery paper obtained an apparent surface for microstructural characterization. Keller's reagents were used as etchants after polishing the specimens as per the standard procedure. Scanning electron microscopy (SEM) investigations were done

with EDX for all the workpieces. Element analysis was carried out to observe the different chemical composition of elements and oxides compounds contents in CSA by EDXRF.

2.4 Hardness Test

A macrohardness tester has been used to evaluate the hardness of the specimens. ASTM: E10 standard used to conduct the experiments. The specimens were well prepared through machining and polishing. Hardness was calculated in Brinell scale, 3000 N load and steel ball having diameter 5 mm indenter for 25 s. Four indentations have been taken at room temperature on the upper surface and an average hardness value was taken.

2.5 Impact Test

The impact test of fabricated specimen was conducted using Charpy impact testing machine as per ASTM: E23 standards. Three specimens for all composition have been made by EDM and the final impact strength value was evaluated by taking the average value of these three specimens.

2.6 Tensile Test

The ultimate tensile strength of developed composite specimen was evaluated with UTM (universal testing machine) loaded with 10KN load. Three cylindrical rod-type specimens for each composition as shown in figure set were prepared as per ASTM: E08 using EDM. The ultimate tensile strength has been obtained at a crosshead speed (2.3 mm/min) by taking the average value.

2.7 Compression Test

The computerized UTM-Auto instrument was used to perform a compression test on these specimens at room temperature. Three specimens for each composition are made according to ASTM: an E9-09 standard to obtain the ultimate compression strength and average value was taken. The compressive strength has been taken precisely because of the machine was fully computerized. A uniform crosshead speed of 1 mm/min was taken during the whole process of evaluation.

2.8 Bending Test

Three point bending test is more realistic rather than compression and tensile test in investigation of reinforced particle in MMCs. The most important explanation was aluminum oxide (Al_2O_3), and SiO_2 (CSA) particulates show the notch effect during the testing. To evaluate the flexural strength three-point bending machine was used with two samples for each composition as per ASTM: A370 standards. A maximum bending load is calculated in this test and flexural strength (MPa) has calculated from the corresponding load. Flexural strength is calculated by the given formula:

$$\sigma = M * y/I \quad (1)$$

where ‘ σ ’ denotes flexural stress, ‘ y ’ is a distance from neutral axis, ‘ M ’ is bending moment, and ‘ I ’ is moment of inertia. In the three-point bend test, peak value of flexural stress occurs at midpoint of the sample.

2.9 Wear Test

A pin-on-disk apparatus is used to examine the dry sliding wear of fabricated specimens. ASTM: G99 standards were taken to conduct the experiments. A steel disk (EN31) of diameter 110 mm was taken to against the slide pin. The cylindrical specimen is prepared of 28 mm in height and 10 mm diameter to study the wear resistance of both composites and base metal (BM) alloy. Various tests were conducted at different loads such as 20 N, 30 N, 40 N, and 50 N at a sliding speed of 3.0 m/s at constant sliding distance of 1500 m at room temperature. The loss of volume (V) was deliberated by calculating the loss in height into the cross-sectional area of the sample pin. Wear rate was calculated using the following Eq. (2).

$$\text{Wear rate} = V/L \left(\text{mm}^3/\text{m} \right) \quad (2)$$

where ‘ L ’ is the sliding distance.

2.9.1 Corrosion Test

The corrosion test was conducted using electrochemical workstation setup as per ASTM: G31- 72 standards. The specimens were prepared by polishing using emery papers and cleaning was done by acetone solution and then washed with water to eliminate unwanted impurities nearby the surface. NaCl (210 g) is mixed with deionized water (6000 cm^3) and the solution was prepared. The three electrodes were used in this method named as (i) the wire electrode of platinum was used as an auxiliary electrode, (ii) electrode of Ag–AgCl used as a reference electrode, and (iii) specimen was used as a working electrode.

3 Results and Discussion

3.1 Microstructural Characterization

The microstructural images for the composites can be clearly seen in Fig. 4a–d. Uniform distribution of dispersed reinforcement particles is visible by the optical images. Figure 4a shows the uniform distribution of micro-segregation (MgZn_2) with fine grains. Porosity levels increase when the content of reinforcement increases which are clearly shown in Fig. 4c, d. The maximum porosity is clearly visible in Fig. 4d.

The uniform distribution of reinforced particles is shown in SEM images for HMMCs which are evident of superior incorporation of hybrid $\text{Al}/\text{Al}_2\text{O}_3/\text{CSA}$ HMMCs. The SEM images of AA7075 alloy Fig. 5a reinforced specimen are clearly shown in Fig. 5b–d. The intermediate phases like $\text{Al}_2\text{Mg}_3\text{Zn}_3$, MgZn_2 , Al_2CuMg , $\text{Al}_{13}\text{Fe}_4$, $\text{Al}_7\text{Cu}_2\text{Fe}$, Mg_2Si , and Al_2Cu might be formed in the solidification period of AA7075 alloy. Figure 5b, c shows the uniform distribution of reinforced Al_2O_3 and CSA particles. It is clearly seen in Fig. 5d when the weight percentage of reinforced particles increases the porosity level.

The SEM with EDX images of AA7075 alloy Fig. 6a and reinforced specimen are clearly shown in Fig. 6b–e. Alumina (Al_2O_3) and coconut shell ash (CSA) reinforced particles phases are successfully developed in AA7075 which was analyzed by SEM with EDX. The presence of (Al, Al_2O_3 , Si, Zn, and Cu) is clearly visible in the major predominant peaks of the graph which confirm the existence of reinforced particles in composite specimens. The reinforced particles act as a barrier where the dislocation movement from one grain to another has to change its direction resulting in increase in ultimate tensile strength. Multidirectional stresses are observed in composite samples than monolithic aluminum due to grain refinement in composite samples with good distribution of reinforcements and low porosity. Selection of process parameters for stir casting acts as a vital

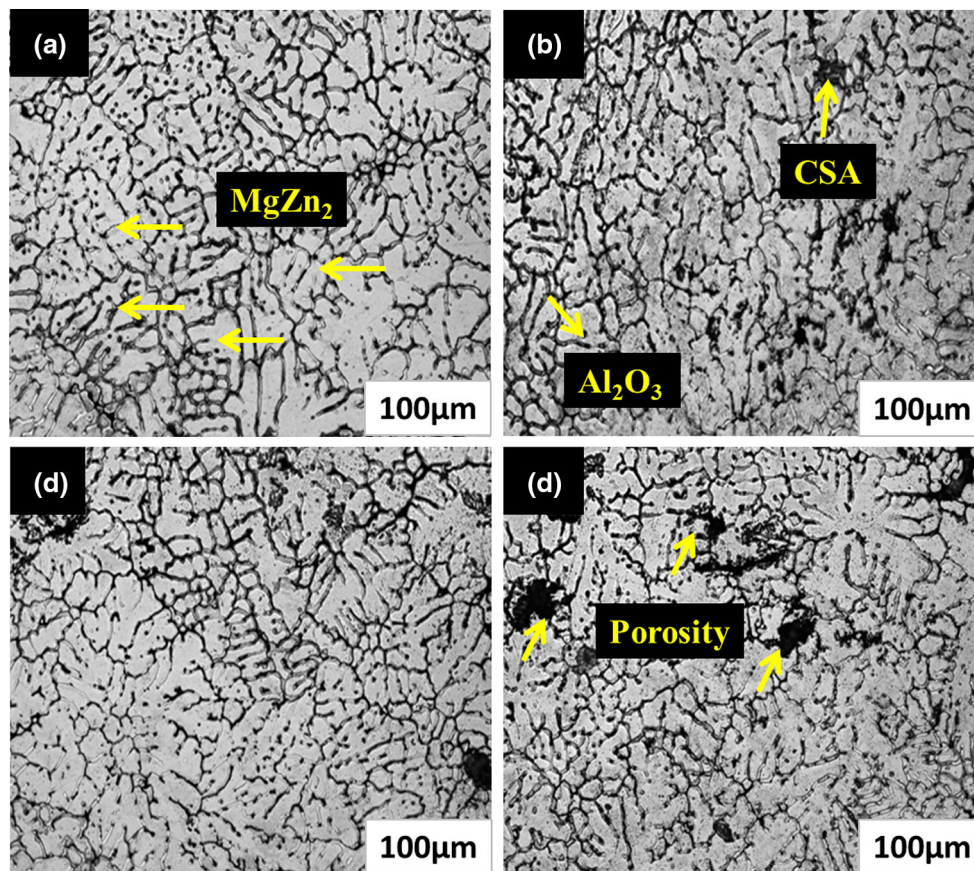


Fig.4 Optical micrographs of: **a** Base AA7075 alloy (N0), **b** HMMC (N1), **c** HMMC (N2), **d** HMMC (N3)

part in homogeneous distribution of reinforcements in the matrix.

The SEM and EDX analyses of the samples are shown in Figs. 5 and 6. The SEM images show uniform distribution of reinforcements for composite samples and are evident for better incorporation of hybrid Al/ Al₂O₃/CSA MMC's. Selection of process parameters for stir casting acts as a vital part in homogeneous distribution of reinforcements in the matrix. Better uniform distribution of reinforcements is achieved at higher temperature. The melting temperature of the particles is higher than molten aluminum, and hence, to reduce clusters high molten temperature is selected in the process. When Al₂O₃ increases, slight clusters can be seen, this is due to thermal mismatch between matrix and reinforcements. The solidification rate is delayed by the hard ceramics when the liquid alloy is surrounded among them which lead to formation of clusters. On the other hand when CSA is increased, fewer clusters are seen since it is a soft ceramic.

3.2 Mechanical Properties

Mechanical properties of hybrid composites increase with addition of B4C and CDA particles. Figure 7 indicates

the hardness of developed AA7075/Al₂O₃/CSA HMMCs increases with reinforcement (CSA and Al₂O₃). The hardness of entire composite was much higher than that of AA7075 alloy. The hardness has been improved for all samples except pure AA7075 due to the presence of Al₂O₃ along with SiO₂ (CSA) particle in matrix material. During indentation, permanent deformation is restricted because of occurrence of Al₂O₃ which solidifies the upper surface. The ductility turns into brittleness when the ceramic particles were put in a metal–matrix which increases the hardness value of HMMCs. The increase in weight % of reinforced particles non-uniformity and non-wettability has been observed and produces the high viscosity of molten metal which causes difficulties in pouring. Uniform distributions of the reinforced particles, density of reinforcement, rate of solidification, and a lesser amount of porosity were few key parameters that influenced hardness of the HMMCs [29]. The resistance toward indentation on reinforced particles was calculated by the BHN value. The optimum hardness value was found to be 85, 98, 138, and 142 BHN for N0, N1, N2, and N3 specimens, respectively. The maximum value was achieved in specimen N3.

Aluminum being a ductile material turns brittle when hard ceramics are added in the matrix which enhances the

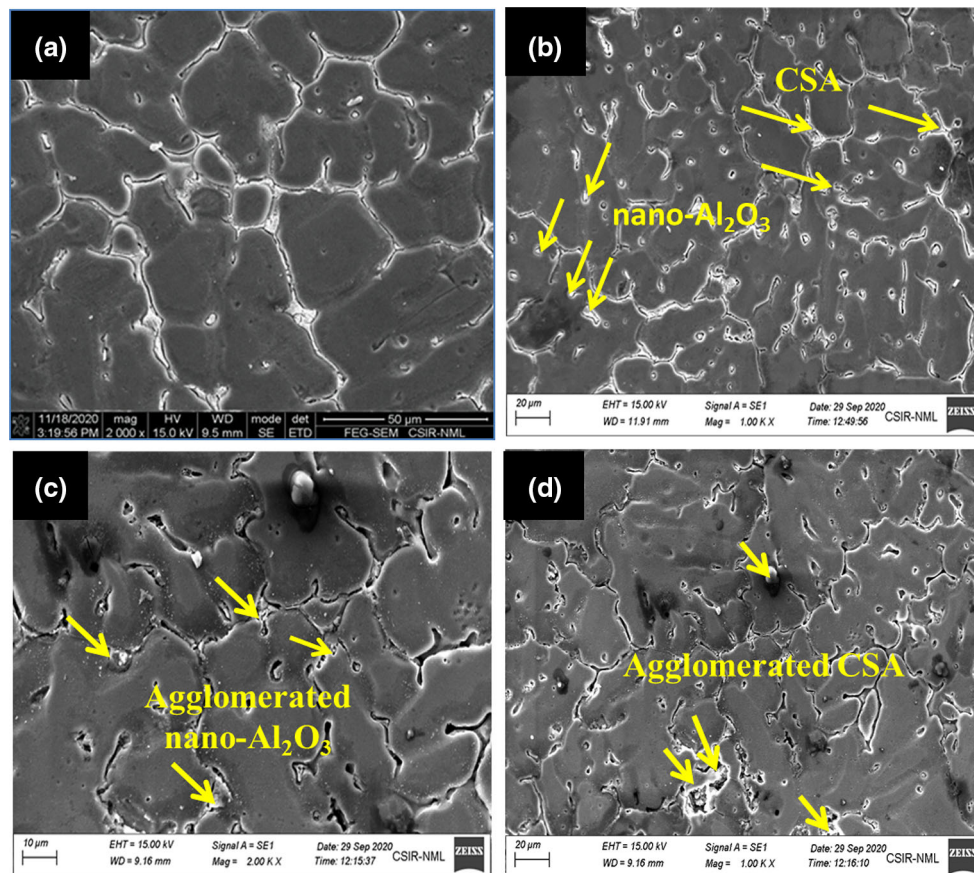


Fig. 5 SEM images of: **a** Base AA7075 alloy (N0), **b** HMMC (N1), **c** HMMC (N2), **d** HMMC (N3)

hardness. Increase in percentage of reinforcements results in non-wettability and non-uniformity in the matrix producing high viscosity which leads to difficulties in pouring the composite material. Uniform distribution of reinforcements, rate of solidification, density of reinforcement particle, and less porosity are few major parameters influencing the hardness of composites [38, 39].

It has been perceived that the impact strength of every fabricated composite specimen is reduced compared with the base AA7075 alloy. Figure 8 indicates the graphical demonstration of average impact strength. The ductile nature of Al-alloy shows high impact energy which experiences the permanent deformation at ambient temperature. The presence of reinforced particles in the composite reduces the impact strength of the entire composite. The brittle nature of hard ceramic particle leads to stress concentration. The uneven dispersal of the reinforcement in matrix material results in formation of the clusters which reduces the bonding between matrix and reinforced particles and decreases the impact strength of HMMCs [30–32]. The resistance toward energy absorption on reinforcement may be recognized by the value of impact strength. The optimum values of impact strength are found to be 3.1, 2.8, 2.4, and 2.21 for N0, N1, N2,

and N3 specimens, respectively. Maximum value of impact strength was found for specimen N0 (AA7075 alloy), shown in Fig. 8.

Figure 9 shows the images of fractographic analysis with SEM for fractured impact specimen. The higher values of impact strength of specimen N0 is due to the presence of more dimple compared to cleavage facet. In the Al-alloy, when the second particles were added, the Al-matrix was transformed from ductile to brittle. The crack initiation and propagation are noticeably seen from Fig. 9a–d. The crack propagation takes place on grain boundaries in the Al-matrix followed by formations of transgranular facet. Stress concentration areas are formed at site of reinforcement particles leading to formation of uneven crack causing poor energy absorption. All over the reinforcement particles, void nucleation can be clearly seen. These initiated crack formations are finally converted into larger cavity. It is also evident from the literature survey that the tensile strength is inversely related to impact strength (i.e., tensile strength increases impact decreases) because of existence of brittleness and uneven cavity in fractured surface.

Figure 10 demonstrates the variation in average ultimate tensile strength (UTS) with varying CSA particles along with

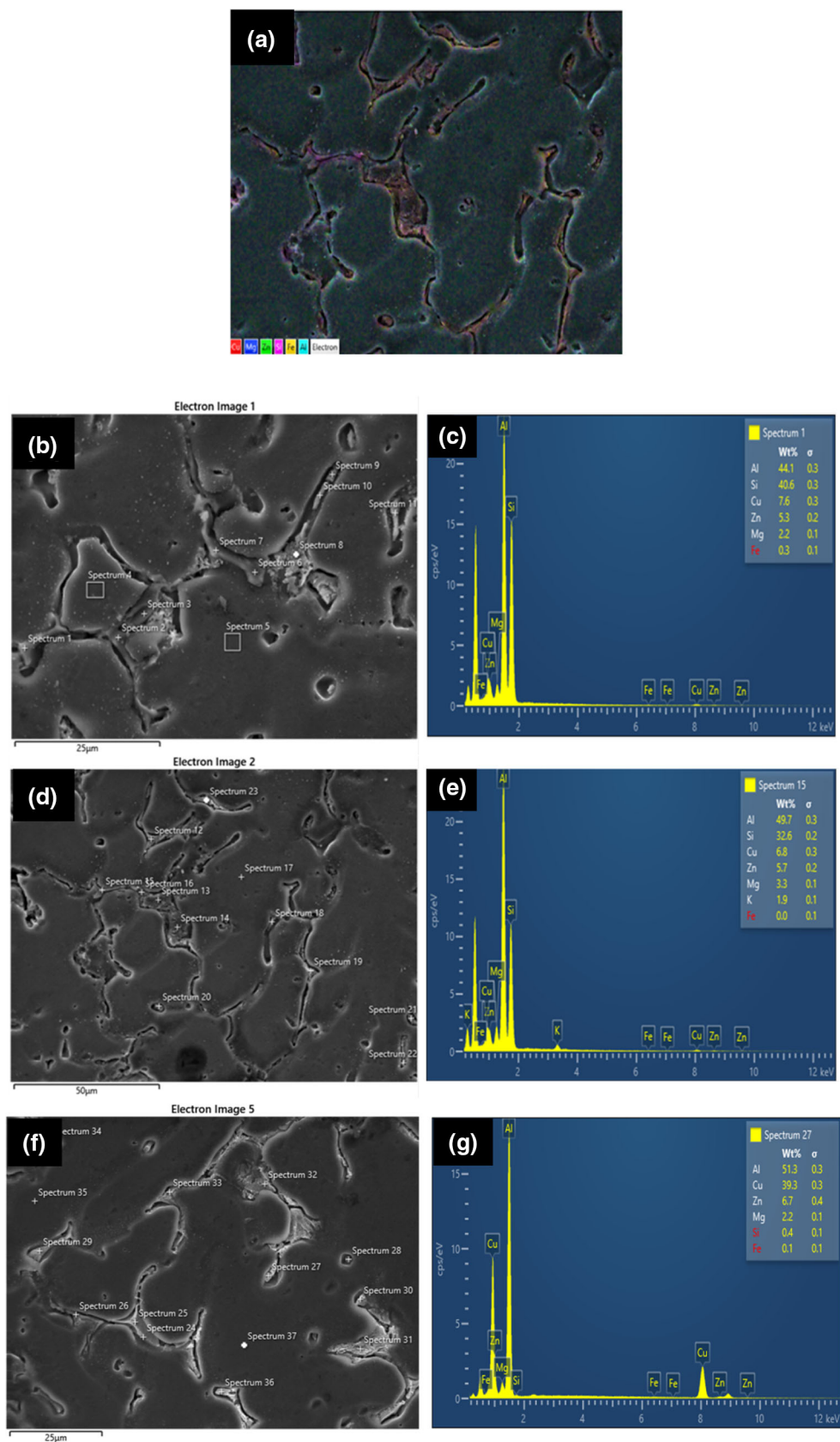


Fig.6 SEM with EDX of: **a** Base metal (N0), **b** HMMC (N1), **c** HMMC (N2), **d** HMMC (N3)

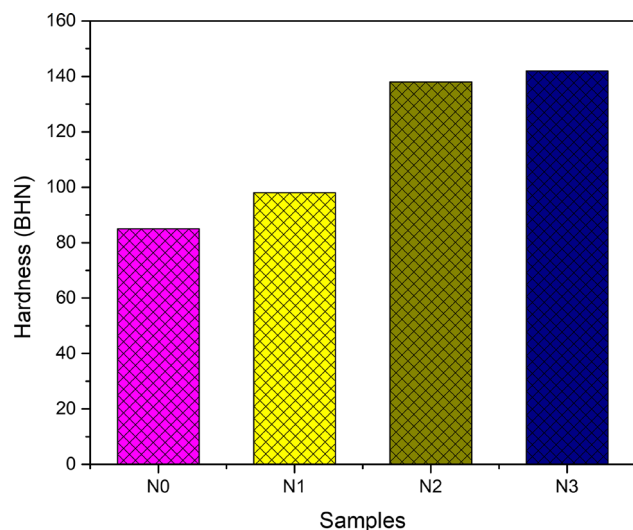


Fig.7 Effect of percentage composition of reinforcement on hardness

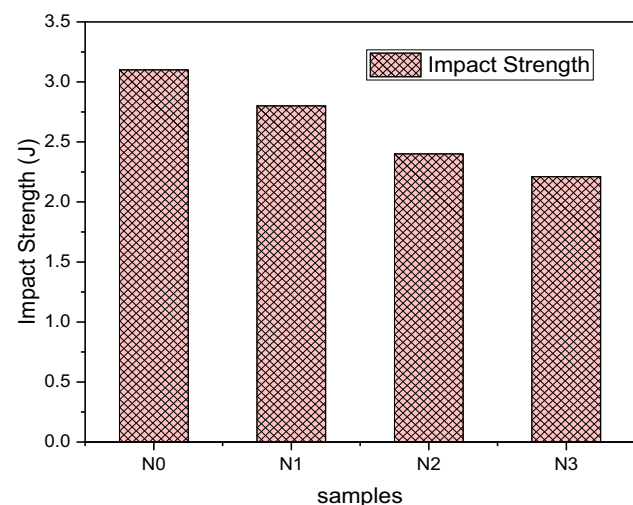


Fig.8 Effect of percentage composition of reinforcement on impact strength

Al_2O_3 particles. The values of UTS were enhanced with weight percentage of CSA content. As increases the Al_2O_3 and SiO_2 (CSA) content, increases the UTS performances mostly due to the stress transference from the matrix material to the reinforcement particles. This is due to the hard reinforcement particles which acts as barrier and restricts generations of the crack propagations which accelerate the dislocations in HMMCs and it is also called as Orowan mechanism [33]. The significant enhancement in the density of dislocation in Al-matrix might be endorsed to enhance the UTS. The adding of Al_2O_3 along with CSA in the Al-matrix leads to increase in grain boundaries. The hindrance in growth of microcracks is created by significant increase in grain boundaries, which in turn enhances the strength. The difference in coefficient of thermal expansion between the

matrix and reinforcement is another reason to generate the geometrical essential dislocations on interface between the matrix and nano-reinforcement during the cooling that can improve strength. Preheating of Al_2O_3 and CSA particles in stir casting will increase interfacial tensile strength and the uniform distribution of reinforced particles in Al matrix. Moreover, the preheating of dispersed particles incites the thermal stress development which influences the UTS in the HMMCs. The coefficient of thermal expansion difference between matrix and reinforcement is also the cause for improvement in the value of UTS. A resistance toward tensile force could be recognized by the value of UTS. The values of average UTS are measured to be 182, 225, 292, and 276 MPa for sample N0, N1, N2, and N3, respectively. The N2 specimen was achieved the highest value when compared to the AA7075 alloy. The variations of yield strength and percentage elongation are also mentioned in Fig. 10. Highest elongation (28.3%) is obtained for N1 and lowest (13%) for N3 sample.

Usually the fracture of tensile specimen is classified into ductile and brittle fracture. Non-homogenous distributions of reinforced particles in Al-matrix and development of secondary phases throughout stir casting are the main aspect which directs the fracture. The uneven dispersal of second particles indicates the difference in the strain carrying capacity between brittle and rigid dispersed particle (Al_2O_3 -CSA) and the ductile AA7075 alloy matrix. The tension fracture investigation of specimen is performed to expose the failure behavior specifically micro-void coalescence and cleavage through FESEM images. The transgranular grain boundary movements in brittle fracture, formed because of a lesser amount of the micro-void coalescence and plastic deformation, are produced in the ductile fracture because of neck formation in specimen. The crack propagations increases due to transgranular facets through micro-voids and grains coalesce together and contribute to crack when the load is larger than the UTS [34, 35].

The variation in UTS with addition of CSA along with nano- Al_2O_3 is shown in Fig. 12. The UTS has been increased for all HMMCs sample when compared with parent AA7075 alloy and the similar facts reported by Embury [36]. This is because the hybrid Al composite has become tougher with the significant addition CSA along with nano- Al_2O_3 particles. It was purposeful till matrix material can lodge the reinforced particles without distortion [37]. CSA and nano- Al_2O_3 reinforced particles are brittle and hard resulting in matrix dispersion hardening. Such reinforced particles act as a secondary phase in matrix alloy and restrict the movements of dislocation and harden the hybrid composite. The average compressive strength values are measured to be 450, 502, 650, and 645 MPa for N0, N1, N2, and N3 specimen, respectively.

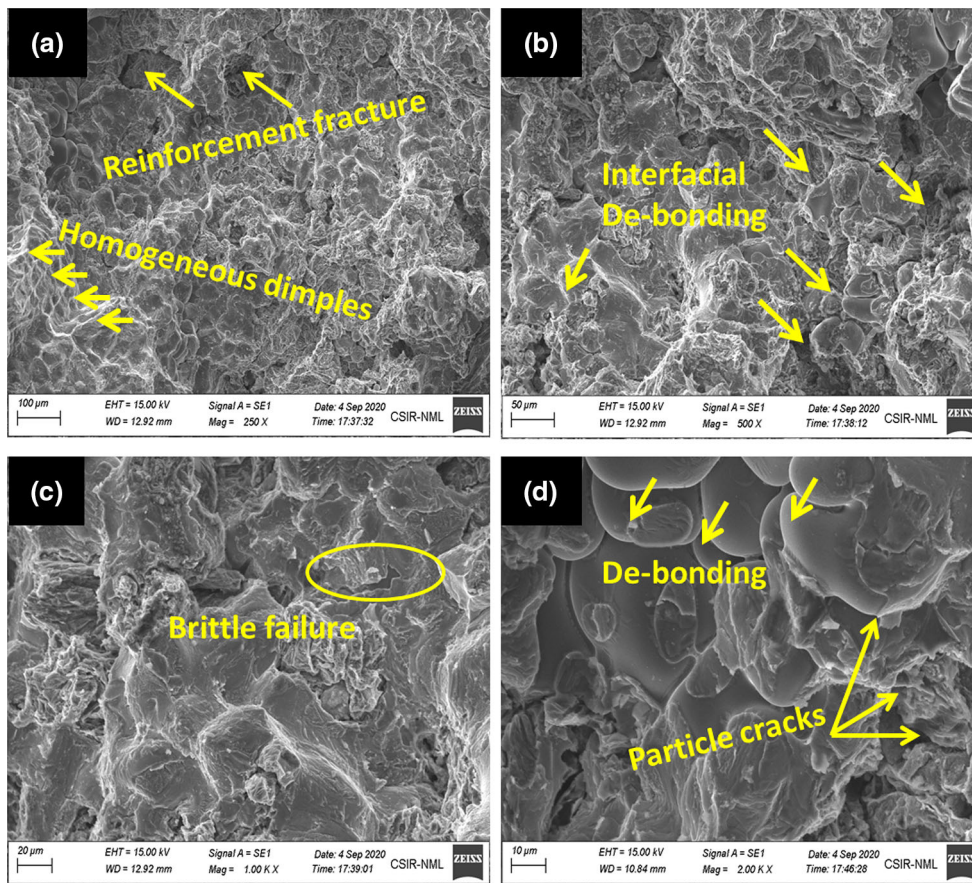
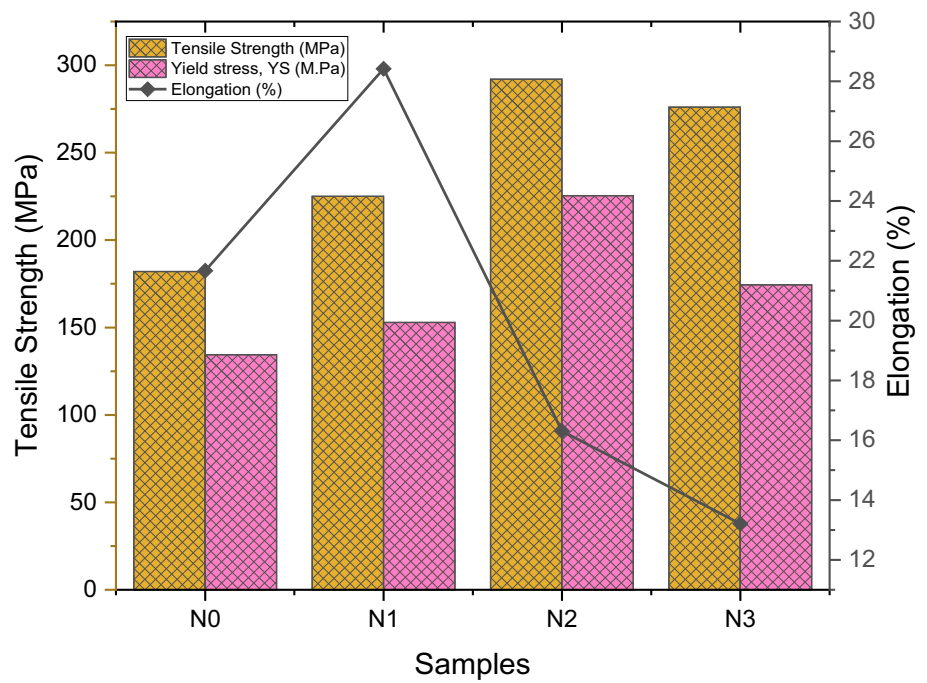


Fig.9 SEM fracture surfaces of casting after impact testing: **a** Base metal (N0), **b** HMMC (N1), **c** HMMC (N2), **d** HMMC (N3)

Fig.10 Effect of percentage composition of reinforcement on ultimate tensile strength and percentage elongation



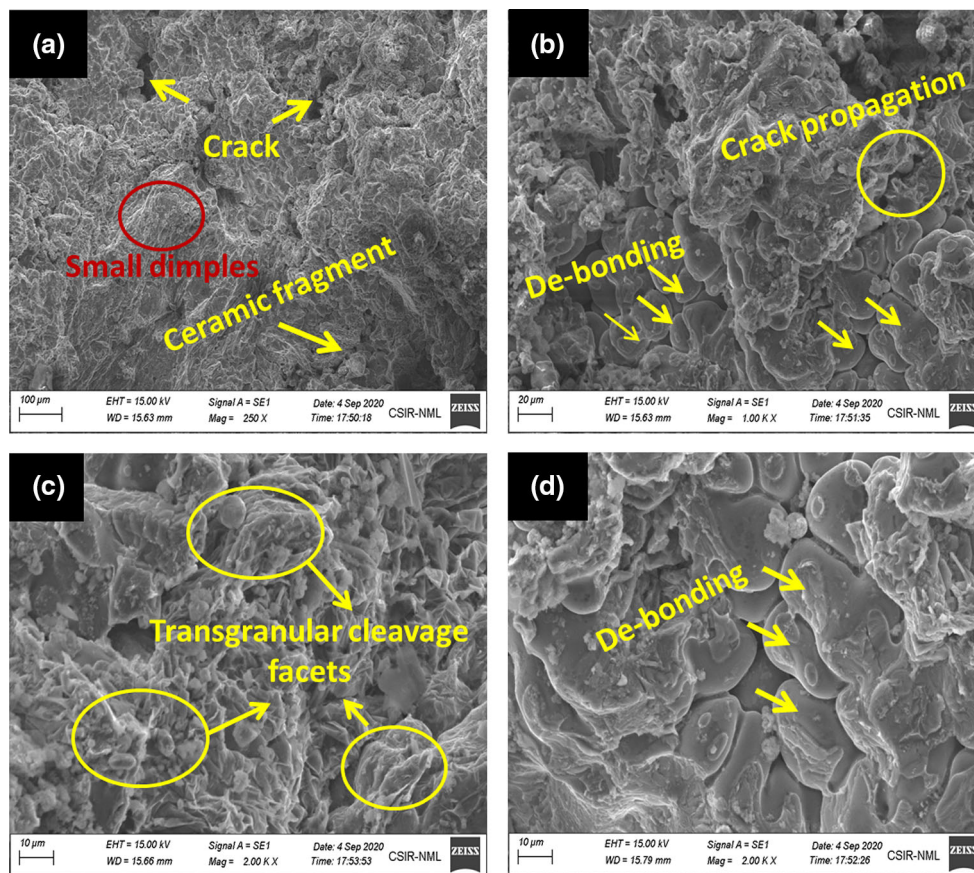


Fig.11 SEM fracture surfaces of casting after impact testing: **a** Base metal (N0), **b** HMMC (N1), **c** HMMC (N2), **d** HMMC (N3)

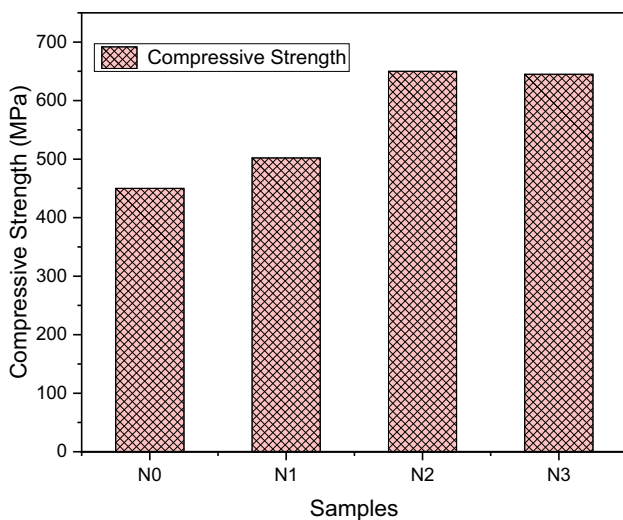


Fig.12 Effect of percentage composition of reinforcement on ultimate compressive strength

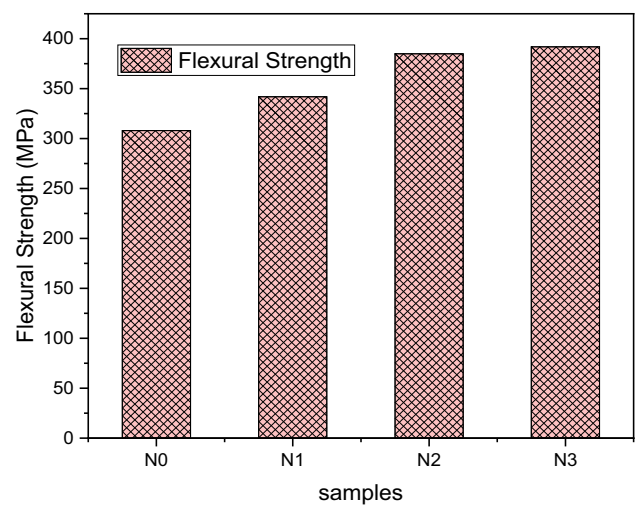


Fig.13 Effect of percentage composition of reinforcement on flexural strength

The effect of variation in reinforcement on flexural strength is shown in Fig. 13. The flexural strength has been enhanced after addition of reinforcement when compare with base Al-alloy. The elastic modulus along with strength of the

specimens was enhanced with addition of reinforcement by preventing dislocation movement which result higher value of flexural strength. The average values of flexural strength are mentioned in Fig. 13. The values of flexural strength

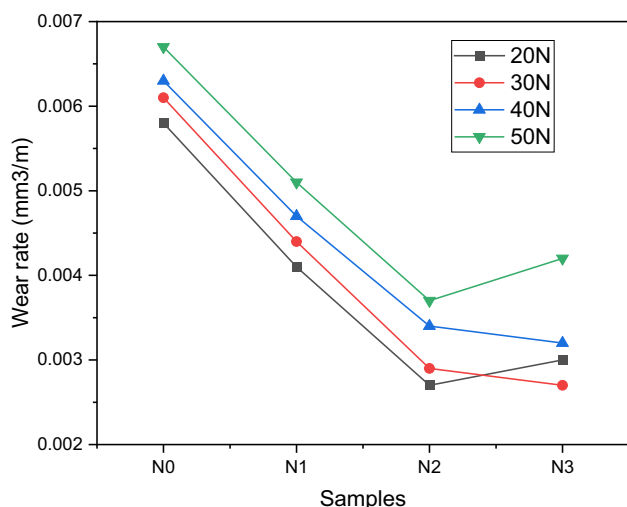


Fig. 14 Effect of percentage composition of reinforcement on wear rate with varying load

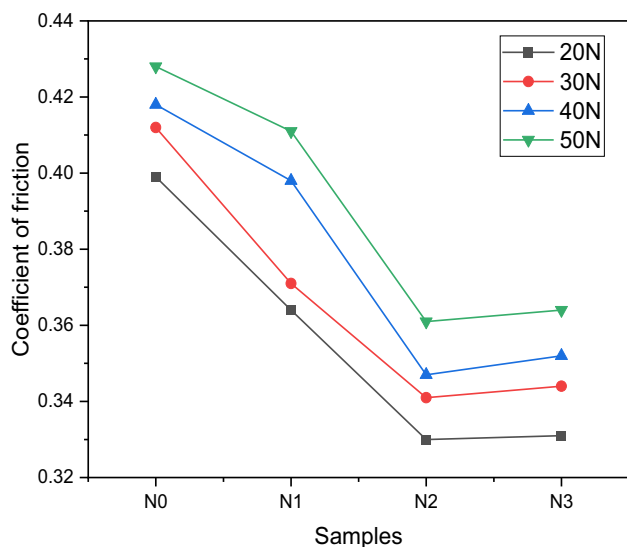


Fig. 15 Effect of percentage composition of reinforcement on coefficient of friction by varying load

enhance for each composite specimen when compared with base Al-alloy.

Figure 14 shows the graphical representation of wear rate variation with second-phase particles, whereas Fig. 15 shows the variation in coefficient of friction with second-phase particles. The coefficient of friction and wear rate were calculated to recognize the composite materials resistance adjacent to sliding surface with the new surfaces. A lesser amount of plastic deformation between the sliding material and a sliding contact area decreases the wear rate. The plastic deformation was achieved because of existence of reinforced particles which reduces the shear stress transfer for the duration of sliding. Through sliding process oxidation of the metallic

particles takes place and the new layer was created on pin surface. During sliding action, a layer formed which experiences distortion, spalling, and fracture. A new layer is formed between a mating surfaces present resistance toward the dilution of contact surfaces [38, 39].

Wear rate gradually decreases for each and every one the composite specimens when compared among the base alloy. The coefficient of friction reduces because of the presence of CSA particles in the HMMCs. The release of soft CSA particles through wearing action performs as a solid lubricant which decreases the value of coefficient of friction. The material removal takes place because of the microscopic removal mechanism in rolling or sliding contact, as the pin surfaces slides on abrasive disk surface. The micro-cutting and micro-plowing phenomena are the main reason of abrasive wear mechanism. From the literature survey, it is concluded that in low wear condition, deformation takes place by means of high wear and micro-plowing condition; deformation takes place due to the micro-cutting mechanism. In HMMCs, the evolution from micro-plowing to micro-cutting mechanism increased the wear resistance against the constant parameters like sliding distance, applied load, and sliding time in the wear test. A little amount of material displacement and greater material removal occurs in high wear material. The material removal takes place in the form of very fine chips because of micro-cutting mechanism and displacement of material takes place in the form of a micro-edge because of micro-plowing mechanism. The high wear is seen in the specimen N0 where there is the absence of reinforced particles. The presence of nano-size hard ceramic (Al_2O_3) and micro-size soft particles (CSA) in the Al matrix has enhanced the wear resistance in the developed composite specimen. The specimen N2 shows a minimum amount of wear compared to other composite specimen.

Figure 16 shows the variation of reinforced particles with different temperatures on corrosion resistance. The corrosion rate gradually decreases with increased weight % of reinforced particles in Al matrix. The sample N0 shows a maximum corrosion rate while compared with developed composite specimens. The surface of specimen gets oxidized as it is introduced into solution prepared. The oxide film on the upper surface of each specimen gets breakdown by the aggressive chloride ions; thus, corrosion produced is greater. The oxide film gets strengthened with the presence of SiO_2 , and thus, further breakdown of layer gets restricted which confine the further corrosion resistance. The corrosion rate gets condensed with increased weight percentage of hard ceramic (Al_2O_3). The varying thermal expansion coefficient across the matrix increases the density of dislocation which can be a cause behind the increased corrosion resistance. High value of hardness coefficient of N3 specimen is the reason behind its minimum corrosion rate. These reinforcements work as barrier which in turn checks the corrosion

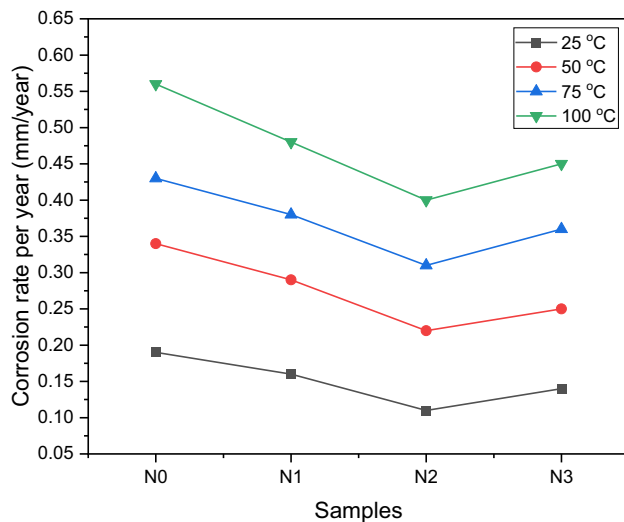


Fig.16 Effect of percentage composition of reinforcement on corrosion resistance

in the composite specimens. The existence of SiO_2 in CSA particles strengthens the oxide film formed on the surface and restricts the oxide breakdown film layer which enhanced the resistance toward corrosion. With increase in weight percentage of hard ceramic (Al_2O_3) particles, the corrosion rate is reduced. The variation in coefficient of thermal expansion among the Al_2O_3 and Al-matrix generates superior dislocation density which is accountable for the growth in corrosion resistance [40, 41]. The minimum corrosion rate is found for N3 specimen due to its high value of hardness. These reinforcements perform as a barrier and restrict the corrosion in each composite specimen.

4 Conclusions

In the current research work, investigations were done to understand the influence of percentage reinforced particles $\text{Al}_2\text{O}_3/\text{CSA}$ in Al-7075 alloy and summarized the following conclusions:

- (i) Optical micrograph and SEM images expose fairly homogeneous dispersion of Al_2O_3 and CSA reinforced particles in Al matrix. SEM with EDX analysis confirms that the reinforcements are present in developed hybrid composite.
- (ii) Hardness of hybrid composite increased while adding Al_2O_3 and CSA reinforced particles in the Al matrix. The maximum hardness value obtained (142 BHN) for sample N3.

- (iii) Impact strength decreases continually with addition of Al_2O_3 and CSA particles for every hybrid composite specimen.
- (iv) The addition of Al_2O_3 and CSA particles increases the ultimate tensile strength of the hybrid composite, while it decreases in the N3 specimen. The maximum value of ultimate tensile strength (292 MPa) was found for N2 specimen.
- (v) Transgranular facet, micro-void coalescence, dimples, and cracks were seen in tensile and impact fractured surfaces.
- (vi) The ultimate compressive strength increases with addition of reinforcements, and it is found that the rate of increment of compressive strength decreases for N3 specimen.
- (vii) It is observed that the flexural strength increases and decreases for different weight % of reinforced particles. The additional amount of CSA particles decreases the value of flexural strength in N3 specimen.
- (viii) Wear rate and coefficient of friction have gradually decreased for every hybrid composite comparing with base metal. Maximum wear resistance was found in N2 specimen.
- (ix) Corrosion rate gradually decreased for every hybrid composite specimen and it was found that the base alloy has maximum corrosion rate.

Acknowledgements The authors appreciate the CSIR-National Metallurgical Laboratory, Jamshedpur, India, for providing the facilities for material characterizations.

Author's contributions Not applicable.

Funding Not applicable.

Availability of data and materials Not applicable.

Declarations

Conflict of interest The authors declare that there is no conflict of interest.

Consent for publication The author signs for and accepts responsibility for releasing this material on behalf of any and all co-authors.

Ethics approval and consent to participate Authors assured and respect the third parties rights such as copyright and/or moral rights.

References

- Mondal, D.P.; Das, S.; Jha, A.K.; Yegneswaran, A.H.: Abrasive wear of Al alloy–Al₂O₃ particle composite: a study on the combined effect of load and size of abrasive. *Wear* **223**, 131–138 (1998)
- Patel, S.K.; Singh, V.P.; Kumar, N.; Kuriachen, B.; Nateriya, R.: Wear behaviour of Al-silicon (LM13) alloy composite reinforcement with TiC and ZrSiO₄ particles. *SILICON* **12**, 211–221 (2020)
- Ikubanni, P.P.; Oki, M.; Adeleke, A.A.: A review of ceramic/bio-based hybrid reinforced aluminium matrix composites. *Cogent Eng.* **7**, 1 (2020)
- Akhil, K.T.; Arul, S.; Sellamuthu, R.: The effect of heat treatment and aging process on microstructure and mechanical properties of A356 aluminium alloy sections in casting. *Procedia Eng.* **97**, 1676–1682 (2014)
- Mohan, K.; Suresh, J.A.; Ramu, P.; Jayaganthan, R.: Microstructure and mechanical behavior of Al 7075–T6 subjected to shallow cryogenic treatment. *J. Mater. Eng. Perform.* **25**(6), 2185–2194 (2016)
- Baradeswaran, A.; Perumal, A.E.: Influence of B₄C on the tribological and mechanical properties of Al 7075–B₄C composites. *Compos. B Eng.* **54**, 146–152 (2013)
- Mobasherpour, I.; Tofigh, A.; Ebrahimi, M.: Effect of nano-size Al₂O₃ reinforcement on the mechanical behavior of synthesis 7075 aluminum alloy composites by mechanical alloying. *J. Mat. Chem. Phys.* **138**, 535–541 (2013)
- Koteswara Rao, V.R.; Chowdary, J.R.; Balaji, A.; Krishna, D.S.; Bhavabhuthi, B.P.; Sreevatsava, G.; Abhiram, K.: A review on properties of aluminium based metal matrix composites via stir casting. *Int. J. Sci. Eng. Res.* **7**(2), 742–749 (2016)
- Kandpal, B.C.; Kumar, J.; Singh, H.: Production technologies of metal matrix composite: a review. *Int. J. Res. Mech. Eng. Technol.* **4**, 27–32 (2014)
- Bhushan, R.K.; Kumar, S.; Das, S.: Fabrication and characterization of 7075 Al alloy reinforced with SiC particulates. *J. Int. Adv. Manuf. Technol.* **65**, 611–624 (2013)
- Sajjadi, S.A.; Ezatpour, H.R.; Torabi-Parizi, M.: Comparison of microstructure and mechanical properties of A356 aluminum alloy/Al₂O₃ composites fabricated by stir and compo-casting processes. *J. Mat. Des.* **34**, 106–111 (2012)
- Toptan, F.; Kilicarlan, A.; Karaaslan, A.; Cigdem, M.; Kerti, I.: Processing and microstructural characterization of AA 1070 and AA 6063 matrix B₄C reinforced composites. *Mater. Des.* **31**, 87–91 (2010)
- Kumar, A.; Singh, R.C.; Chaudhary, R.; Singh, V.P.: Tribological studies and microstructural characterisation of SiC and fly ash particles based aluminium 2024 alloy composites prepared through stir casting route. *IOP Conf. Ser. Mater. Sci. Eng* (2020) 804012025.
- Rao, V.R.; Ramanaiah, N.; Sarcar, M.M.: Tribological properties of aluminium metal matrix composites (AA7075 reinforced with titanium carbide (TiC) particles). *Int J Adv Sci Technol* **88**, 13–26 (2016)
- Radhika, N.; Raghu, R.: Investigation on mechanical properties and analysis of dry sliding wear behavior of Al LM13/AlN metal matrix composite based on Taguchi's technique. *J Tribol* **139**(4), 041602 (2017)
- Baradeswaran, A.; Perumal, A.E.: Wear and mechanical characteristics of Al7075/graphite composites. *Compos. B Eng.* **56**, 472–476 (2014)
- Alaneme, K.K.; Akintunde, I.B.; Olubambi, P.A.; Adewale, T.M.: Fabrication characteristics and mechanical behaviour of rice huskash–Alumina reinforced Al–Mg–Si alloy matrix hybrid composites. *J. Mater. Res. Technol.* **2**(1), 60–67 (2013)
- Bhandakkar, A.; Prasad, R.C.; Sastry, S.M.: Fracture toughness of AA2024 aluminum fly ash metal matrix composites. *Int. J. Compos. Mater.* **4**(2), 108–124 (2014)
- Manikandan, R.; Arjunan, T.V.; Akhil, O.P.; Nath, R.: Studies on micro structural characteristics, mechanical and tribological behaviours of boron carbide and cow dung ash reinforced aluminium (Al 7075) hybrid metal matrix composite. *Compos. Part B-Eng.* **183**, 107668 (2020)
- Rohatgi, P.K.; Daoud, A.; Schultz, B.F.; Puri, T.: Microstructure and mechanical behavior of die casting AZ91D-Fly ash cenosphere composites. *Compos Appl Sci Manuf* **40**(6–7), 883–896 (2009)
- Patel, S.K.; Nateriya, R.; Kuriachen, B.; Singh, V.P.: Effect of secondary phase particles on Erosive wear characteristic of dual reinforced particle Al-alloy composites. *Mater Today* **5**(9), 17561–17571 (2018)
- Mazahery, A.; Abdizadeh, H.; Baharvandi, H.: Development of high-performance A356/nano-Al₂O₃ composites. *J. Mat. Sci. Eng. A* **518**, 61–64 (2009)
- Nguyen, Q.B.; Gupta, M.: Enhancing compressive response of AZ31B using nano-Al₂O₃ and copper additions. *J. Alloys Compd.* **490**, 382–387 (2010)
- Akbari, M.K.; Baharvandi, H.R.; Mirzaee, O.: Fabrication of nano-sized Al₂O₃ reinforced casting aluminum composite focusing on preparation process of reinforcement powders and evaluation of its properties. *Compos. Part B-Eng.* **55**, 426–432 (2013)
- Patel, S.K.; Nateriya, R.; Kuriachen, B.; Singh, V.P.: Slurry abrasive wear, microstructural and morphological analysis of titanium carbide and zirconium sand aluminium alloy (A5052) metal matrix composite. *Mater. Today* **5**(9), 19790–19798 (2018)
- Escalera-Lozano, R.; Gutierrez, C.A.; Pech-Canul, M.A.; Pech-Canul, M.I.: Corrosion characteristics of hybrid Al/SiCp/MgAl₂O₄ composites fabricated with fly ash and recycled aluminum. *Mater. Char.* **58**(10), 953–960 (2007)
- Subramaniam, B.; Natarajan, B.; Kaliyaperumal, B.; Samuel Chelladurai, S.J.: Investigation on mechanical properties of aluminium 7075–boron carbide–coconut shell fly ash reinforced hybrid metal matrix composites. *China Found.* **15**, 449–456 (2018)
- Kim, S.W.; Kim, D.Y.; Kim, W.G.; Woo, K.D.: The study on characteristics of heat treatment of the direct squeeze cast 7075 wrought Al alloy. *Mater. Sci. Eng. A* **304**, 721–726 (2001)
- Baradeswaran, A.; Vettivel, S.C.; Perumal, A.E.; Selvakumar, N.; Issac, R.F.: Experimental investigation on mechanical behaviour, modelling and optimization of wear parameters of B₄C and graphite reinforced aluminium hybrid composites. *Mater. Des.* **63**, 620–632 (2014)
- Balasubramanian, I.; Maheswaran, R.: Effect of inclusion of SiC particulates on the mechanical resistance behaviour of stir-cast AA6063/SiC composites. *Mater. Des.* **65**(5), 11–20 (1980–2015)
- Fadavi Boostani, A.; Tahamtan, S.; Jiang, Z.Y.; Wei, D.; Yazdani, S.; Azari Khosroshahi, R.; Taherzadeh Mousavian, R.; Xu, J.; Zhang, X.; Gong, D.: Enhanced tensile properties of aluminium matrix composites reinforced with graphene encapsulated SiC nanoparticles. *Compos. Part A Appl. Sci. Manuf.* **68**, 155–163 (2015)
- Nam, T.H.; Requena, G.; Degischer, P.: Thermal expansion behaviour of aluminum matrix composites with densely packed SiC particles. *Compos. Part A Appl. Sci. Manuf.* **39**(5), 856–865 (2008)
- Surappa, M.K.; Prasad, S.V.; Rohatgi, P.K.: Wear and abrasion of cast Al-alumina particle composites. *Wear* **77**, 295–302 (1982)
- Ozden, S.; Ekici, R.; Nair, F.: Investigation of impact behaviour of aluminium based SiC particle reinforced metal–matrix composites. *Compos. Part A Appl. Sci. Manuf.* **38**(2), 484–494 (2007)
- Yadav, P.K.; Patel, S.K.; Singh, V.P.; Verma, M.K.; Singh, R.K.; Kuriachen, B.; Dixit, G.: Effect of different reinforced metal-matrix



- composites on mechanical and fracture behaviour of aluminium piston alloy. *J. Biol. Tribol. Corros.* **7**(54), 1–12 (2021)
36. Embury, J.D.: Plastic flow in dispersion hardened materials. *Metall. Mater. Trans. A* **16**, 2191–2200 (1985)
37. Mcdanels David, L.: Analysis of stress–strain fracture and ductility behaviour of aluminium matrix composites containing discontinuous silicon carbide reinforcement. *Metall. Mater. Trans. A* **16**, 1105–1115 (1985)
38. Yadav, P.K.; Dixit, G.; Dixit, S.; Singh, V.P.; Patel, S.K.; Purohit, R.; Kuriachen, B.: Effect of eutectic silicon and silicon carbide particles on high stress scratching wear of aluminium composite for various testing parameters. *Wear* **482–483**, 203921 (2021)
39. Urena, A.; Rams, J.; Campo, M.; Sanchez, M.: Effect of reinforcement coatings on the dry sliding wear behaviour of aluminium/SiC particles/carbon fibres hybrid composites. *Wear* **266**(11–12), 1128–1136 (2009)
40. Loto, R.T.; Babalola, P.: Corrosion polarization behaviour and microstructural analysis of AA1070 aluminium silicon carbide matrix composites in acid chloride concentrations. *Cogent Eng.* **4**(1), 1422229 (2017)
41. Albiter, A.; Contreras, A.; Salazar, M.; Gonzalez- Rodriguez, J.G.: Corrosion behaviour of aluminium metal matrix composites reinforced with TiC processed by pressureless melt infiltration. *J. Appl. Electrochem.* **36**(3), 303–308 (2006)

